Article

Study on Slope Monitoring and Stability Based on Bolt–Cable Combined Support

Yun Liu [1], Jie Lai [1] and Jiangbo Xu [2,*]

[1] Xi'an Research Institute of High-Tech, Xi'an 710025, China; liuyun_1988@yeah.net (Y.L.); dadalai1234@sina.com (J.L.)
[2] School of Highway, Chang'an University, Xi'an 710064, China
* Correspondence: xujiangbo@chd.edu.cn

Abstract: To provide reference for the design and construction of anchoring measures in slope reinforcement and treatment projects, this article presents the on-site monitoring and analysis of the stress changes in anchor rods and anchor cables in a high-level layered rock slope of a deep excavation highway. Anchor rods and anchor cables are widely used reinforcement measures in slope reinforcement due to their simplicity and economy. In this article, we took the layered rock slope of a deep excavation highway as the monitoring object and installed monitoring equipment on slopes of different levels. Based on the monitoring data of slope anchor rods and anchor cables, the rationality of slope reinforcement and treatment measures was analyzed. This study shows that active support anchor cables have better reinforcement effects than the passive protection of anchor rods. The approximate position of the potential slip surface in the slope mass can be inferred according to the monitoring of slope anchor stress, which can guide a slope reinforcement and treatment project. Finally, FLAC3D V6.0 was used for numerical simulation analysis, which showed that the slope was in a stable state under the support of anchor rods and anchor cables.

Keywords: slope; slope protection; slope anchor monitoring; anchor rod stress monitoring; anchor cable stress monitoring

1. Introduction

With the continuous construction of high-grade highways such as expressways, construction projects such as deep excavation highway cuttings and high embankments are gradually becoming more widespread in road construction projects of various grades. However, with the increasing number of slope instability incidents associated with the high embankment and deep excavation of roadbeds, the frequency of accidents is also on the rise. These slope instability accidents not only seriously affect the normal operation of a transportation system but also bring about significant economic losses and even endanger the safety of drivers and pedestrians, resulting in serious social impacts.

Therefore, to prevent accidents such as slope instability, various reinforcement and protection measures are taken in slope engineering, and anchoring measures such as anchor rods and anchor cables are common slope reinforcement measures. A large number of scholars at home and abroad have conducted in-depth research in the field of slope stability monitoring. Xu Yongfu [1] studied expansive soil landslides and divided and their protection techniques into three types, separation protection, support protection, and reinforcement protection, and conducted research on them. Wang Linfeng [2] proposed a plate spring vibration damping anchor head structure and implementation plan that combines excellent seismic resistance and toughness to address the problem of "no toughness" and "poor toughness" in the anchor cable system of high and steep slopes under earthquake sliding. Zhang Li [3] adopted a combination of theoretical analysis, numerical simulation, and on-site testing to study the deformation characteristics and anti-slide mechanism of

micro pile foundations and proposed corresponding anti-slide design schemes. Meng Ziyao [4] adopted the method of reinforcing slopes with anchor rods and predicted the axial force of the anchor rods based on the ACO-SVM model. Huang Yu [5] conducted numerical simulation of a slope dynamic response based on pile anchor support structure and verified the stability of the slope using Newmark slider analysis. Yang Jianhui [6] first proposed a finite element calculation method for the internal force of the slope-anchoring frame which can reflect frictional resistance, axial load, and simplify the anchor rod to equal force. Song Minggang [7] derived expressions for interface shear and axial stress in anchor structures based on the shear lag model and established a mathematical model for prestressed coupling and decoupling. Based on the calculation of three-dimensional anchoring force and the modified differential evolution algorithm, combined with the spatial distribution of three-dimensional anchoring force, Yin Zhikai [8] optimized the anchoring position of the three-dimensional slope to achieve the goal of saving the number of anchor rods. Yan Zhixin [9] analyzed the force interaction, anchoring force transmission, and anchoring effect of anchored slopes under seismic loads through shaking table model tests. On the basis of existing support, Chen Xiuqing [10] reinforced the upper slope with reinforced concrete frame mesh and anchor cables and the lower slope with cross beam anchor cables for secondary reinforcement. Wang Qiuyi [11] used high-strength material BFRP as the anchoring structure and compared the dynamic response of slopes with and without a BFRP structure under different conditions through FLAC3D numerical simulation. Feng Jincai [12] proposed a new method for slope safety warning based on the internal force of anchor bolts in anchoring structures. Xu Xi [13] used a pseudostatic analysis method to analyze the stability of pile anchor reinforcement slope at the foot of the slope, based on the instability caused by factors such as rainfall at the foot of the slope. Xu Yongfu [14] developed a standardized design and construction process for geotextile woven bag prevention and control technology applicable to expansive soil slopes. Wang Wuchao [15] conducted orthogonal experiments using FLAC3D to study the slope-anchoring mode, and the results showed that the improved pile element can better simulate the slope-anchoring mode. In order to improve the stability of the slope in the scenic area, Gao Bingli [16] proposed comprehensive remediation measures such as the demolition of blocks, drainage, spraying, and avoidance, which achieved good results. Yan Changgen [17] summarized the Loess slope protection technology, pointed out the shortcomings of traditional protection technology, and looked forward to the future of ecological vegetation slope protection. Li Danfeng [18] used a three-dimensional finite element simulation method to study the synergistic mechanism of pile group and anchor rod composite structures under traffic loads. Yan Zhixin [19] used FLAC3D to obtain the distribution pattern of shear stress at the anchorage interface under seismic loads and analyzed the effects of factors such as seismic parameters and anchorage forms on shear stress. Nguyen [20] used numerical modeling for slope stability analysis under the impact of rainfall for the Janina mine waste dump, located in Libiąż, Poland, and the authors found that slope tends to lose stability in cases of high rainfall intensity and short duration. Di Maio [21] obtained a deeper insight in the slow and continuous movements of a deep and complex active landslide system which caused severe damage to Latronico by means of both ground-based displacement measurements. Dong [22] separated the aging component of the slope displacement using the empirical mode decomposition method and proposed a parameter back-analysis method based on the aging displacement increment of the slope. Saurabh [23] made an attempt to study the influence of jute fiber reinforcement with the help of three case studies. Tiwari [24] carried out stability analyses of these rock slopes by using numerical programs and simulated the proposed slope profile with several berms between successive foundations in the numerical model. Chen [25] studied two failure cases of a high-cut slope in the Northeastern Area of Sichuan, China. Urbański [26] presented a successful stabilization action of a building structure in an active landslide using the history of the case and a FEM simulation. Arbanas [27] used modelling techniques to create an MRMM which was refined through their use on over forty mining projects that ranged from green field studies to mature producing mines.

Domestic and foreign scholars have only conducted research on slope protection with a single anchor rod or anchor cable, and there is insufficient research on the protective effect of the combination of them on slopes. To study the effectiveness of a certain slope-anchoring measure and the stability of a slope, this paper focuses on a high-speed project's deep excavation of the high slope section in the cutting area from K49 + K840 to K50 + 010. The structural internal force changes in anchor rods and anchor cables during the excavation process and after excavation completion will be monitored to analyze the slope stability. Additionally, FLAC3D numerical simulation software will be employed to assess the reliability of the support scheme and the stability of the slope based on shear strain increments and displacement changes.

2. Project Overview

The Luanxian to Lushi Expressway is an important component of the "Double Thousand Project" in Henan Province, with a total length of 75 km. The construction of this expressway project can greatly alleviate the traffic situation in Sanmenxia City and has significant value for regional economic development. The expressway of Luanxian County is shown in Figure 1. The expressway project is mainly located in the western mountainous and hilly area of Henan Province, in the eastern section of the Qinling Mountains. The terrain is generally higher in the southwest and east, and lower in the northwest, with the southern part being the Funiu Mountain area and the Xionger Mountain area located to the south and west. The terrain is characterized by large fluctuations, continuous peaks and valleys, steep mountain slopes, and the lowest ground elevation of 700 m and the highest of 2192 m. The mountainous terrain is steep, and the construction sections are mainly rock excavation.
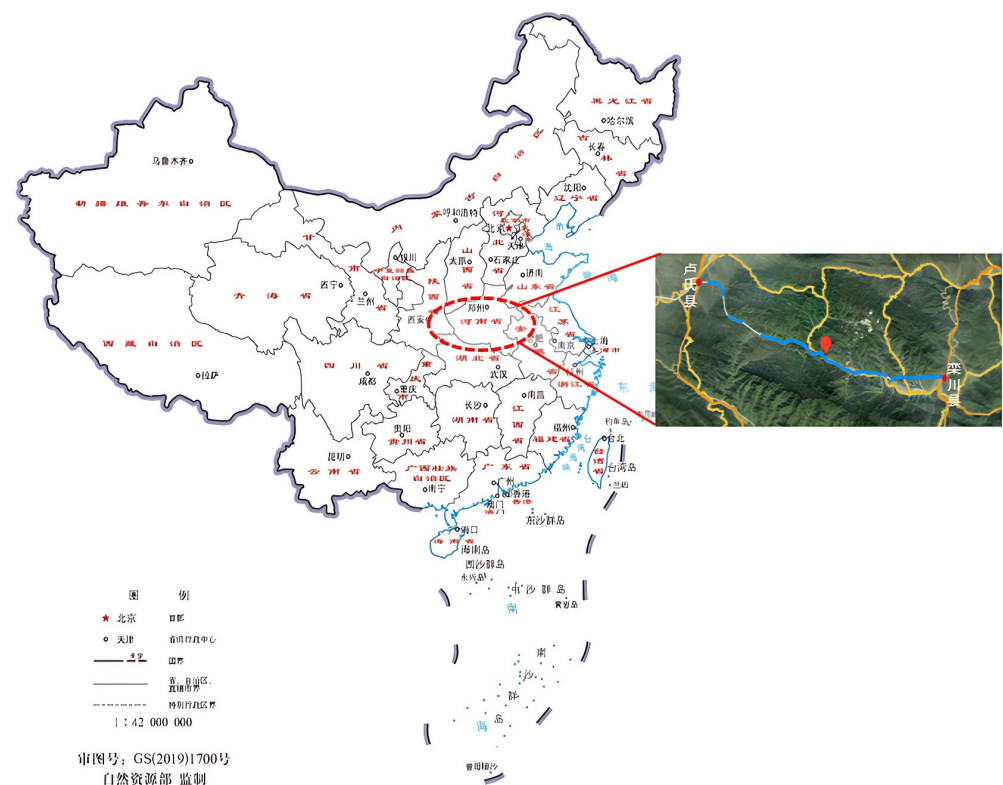

Figure 1. Plan of Luanxian Expressway.

The deep excavation cutting section is located between mileposts K49 + 840 to K50 + 010. Figure 2 shows a cross-section of the slope. In this construction segment, excavation was conducted on both sides of the road. The maximum height of the slope was 65.6 m, and the length of the slope segment was 170 m. The natural slope gradient at the location where the road crosses was approximately 42°.
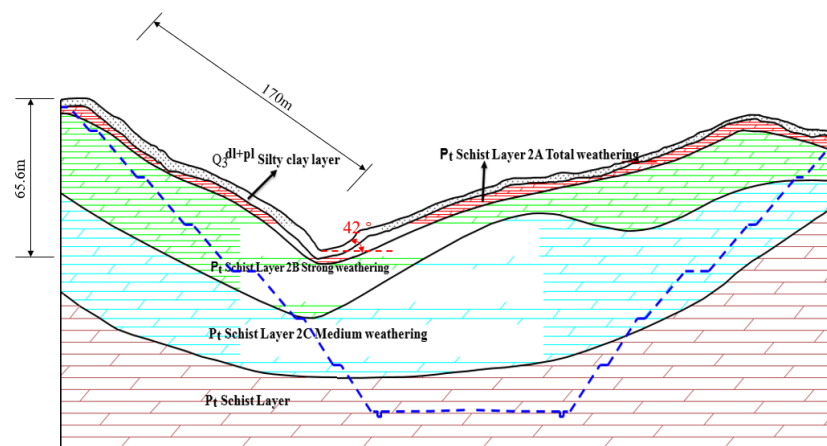
Figure 2. ZK49 + 930.00 Cross-Section of the Slope.

The slope of the road cut exhibited minor tensile fractures along joints, with mudstone fill and poor bonding at the joint interfaces. The rock mass remained intact, with outward dipping structural planes primarily consisting of joint fissures. The slope inclination coincided with the orientation of the underlying bedrock, indicating a parallel-layered slope comprising mainly schist rock with homogenous lithology. According to Appendix E of the *Design Specifications for Highway Subgrades (JTG D30-2015)*, this slope falls under Type IV (Supplementary Materials). Table 1 presents the physical and mechanical properties of each rock layer comprising this rocky slope.

Table 1. Geotechnical Parameters of the Slope.

Rock Layer	Density, kg/m^3	Deformation Modulus, E/MPa	Poisson Ratio	Cohesion, KPa	Internal Friction Angle, KPa
Fully weathered schist	2580	1500	0.35	50	26
Strongly weathered schist	2720	1700	0.32	70	30
Moderately weathered schist	2820	2000	0.28	100	35

The excavated area within the exploration depth range mainly consisted of Precambrian schist (Pt). The geomorphic unit of the excavation area belonged to the Zhongshan Landform, characterized by uneven terrain with a higher elevation on the right side and a lower elevation on the left. The mountainous terrain is steep, with developed nearby valleys having a V-shaped morphology. The slopes of the mountains are covered by dense vegetation with well-developed root systems, providing good natural slope stability. However, excavation of the slope has resulted in the redistribution of stress within the mountain, leading to stress concentration at the foot of the slope. The presence of pore water pressure in the slope, particularly during periods of heavy rainfall, increased the weight of the slope, resulting in a significant reduction in the shear strength of the slope's rock and soil structure. As a consequence, the slope may experience collapse or sliding deformation along a relatively weak plane (such as a parallel joint plane or a weathered interface) due to stress concentration and insufficient shear strength. Therefore, necessary reinforcement measures must be taken to ensure the overall stability of the slope.

It is practically impossible for pre-excavation exploration to fully reveal the engineering geological characteristics of a slope. Moreover, during the excavation and anchoring process, the slope will inevitably be subjected to disturbances from both natural and human factors. For rock and soil slopes, timely anchoring after excavation is beneficial for preserving the inherent strength of potential sliding planes and fully utilizing the self-stabilizing ability of the slope to ensure its stability and safety. Therefore, it is highly necessary to adopt

a dynamic design approach and implement continuous monitoring measures throughout the entire process of slope excavation and anchoring, so as to promptly grasp the stress conditions of the slope anchoring and ensure the long-term stability of the slope.

3. Anchoring and Monitoring Plan for Slopes

The left cut slope section of deep excavation in ZK49 + 820.00~ZK49 + 970.00 of this highway project had a natural slope height of 64.5 m, which increased to 65.1 m after construction, and due to excavation, the potential sliding surface of the slope was located at the weak interlayer. The slope was divided into seven levels, with the seventh level having a height of 5.1 m and the remaining six levels having a height of 10 m each. The slope ratio was 1:0.75 for the first and second levels and 1:1 for the rest. The first, second, and fifth levels were protected with anchor rod framework beams, the third and fourth levels were protected with anchor cable framework beams, the sixth level was protected with a zigzag skeleton, and the seventh level was protected with a three-dimensional net and vegetation.

Due to the high tensile strength and strong deformability of anchor rods or cables, they can effectively solve the problem of tensile fractures in the slope of a road. This article investigates the monitoring results for anchor rods and anchor cables in the section ZK49 + 820.00~ZK49 + 970.00, which is a section with deep excavation. The most representative slope, in section K49 + 930.00 of the left slope cut, was selected for analysis. In the first and fifth levels, the lowest two anchor rods were each equipped with YT-ZX-0400 series vibrating wire strain gauges at three positions over depths (namely at 3 m, 6 m, and 9 m). In the third and fourth levels, all three anchor cable-anchoring positions were equipped with YT-ZX-0400 series vibrating wire anchor cable gauges. The monitoring plans for each level of slope are shown in Figure 3. The anchor cable was a 10 m prestressed anchor cable with a diameter of 15 cm. The length of the anchoring section exceeded 3 m, with a yield strength of 1650 Mpa and a design load of 500 kN. The anchor rod was a 10 m non prestressed anchor rod with a design load of no less than 120 kN.
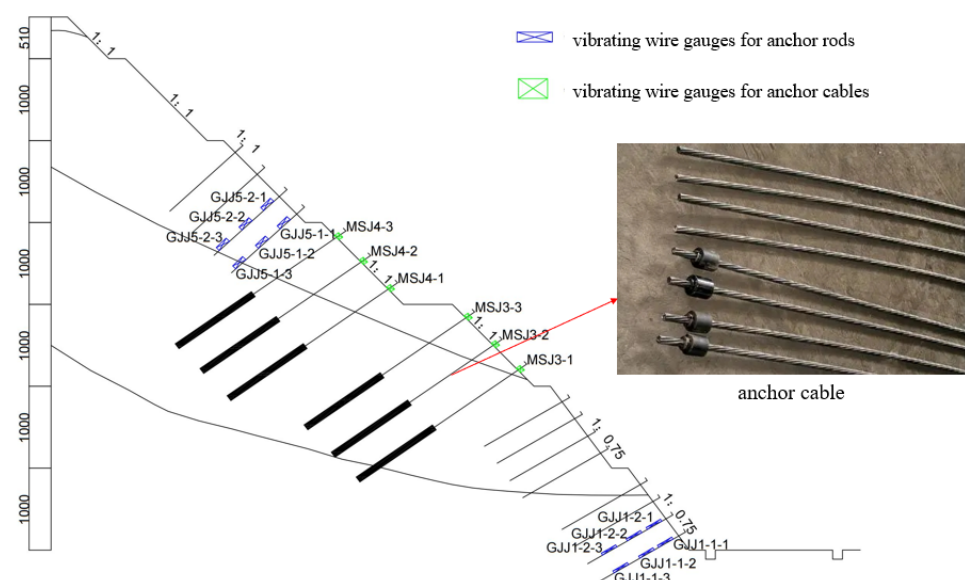

Figure 3. Anchoring and Monitoring Layout Plan for Slope Section K49 + 930.00.

4. Analysis of the Stress Monitoring Results of the Slope

Figures 4 and 5 show the stress changed in anchor 1 and anchor 2 located on the fifth-level slope, respectively. Both show an increasing trend over time until reaching a stable stress value. During the slope protection construction and stable operation stages, the maximum stress of anchor #1 was located in the middle section at a depth of 6 m, with a maximum load stress of 109 kN. The maximum stress of anchor #2 was also located in the middle section at a depth of 6 m, with a maximum load stress of 85 kN. The test results of

the load stress of the anchor at different depths indicate that the 12 m long fully bonded anchor's maximum stress occurred at a depth of approximately 6 m, where a potential sliding surface existed.
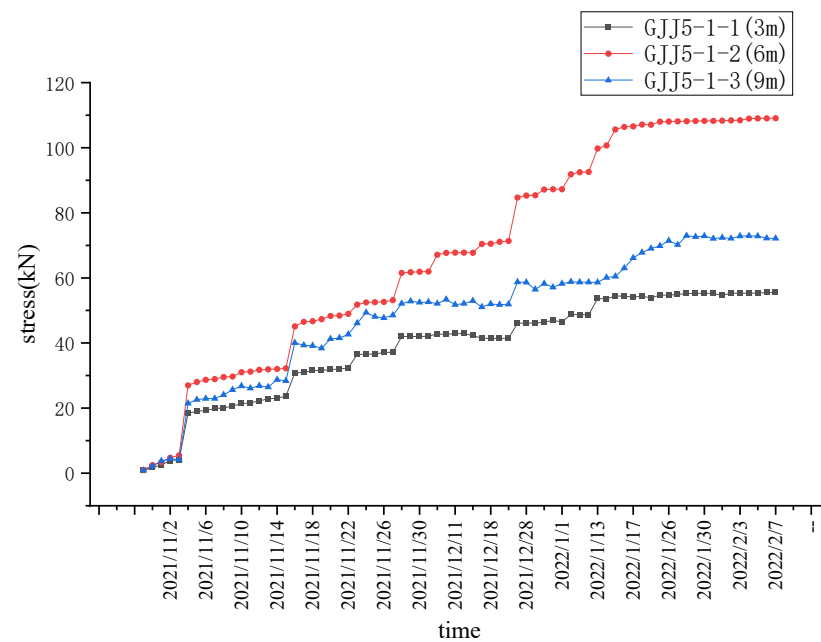

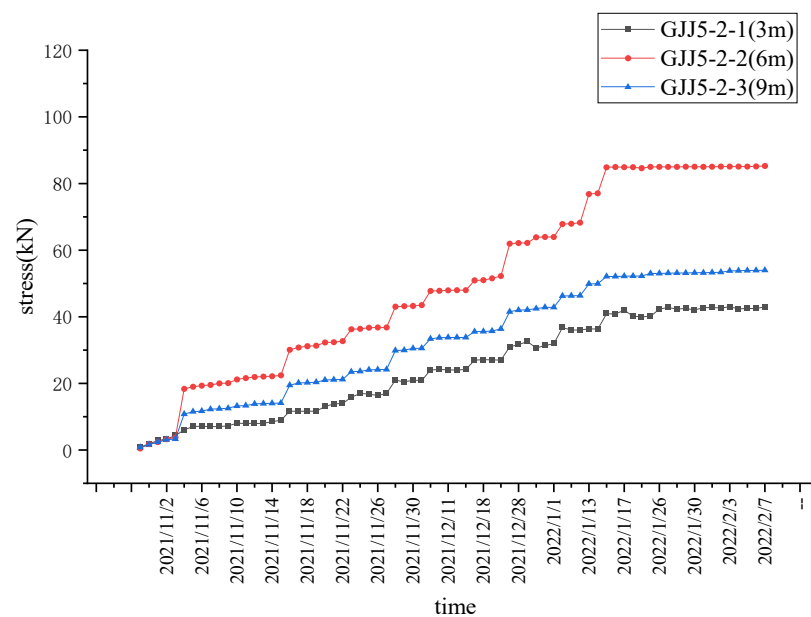**Figure 4.** No. 1 Anchor Rod of the Fifth Slope.

Figure 5. No. 2 Anchor Rod of the Fifth Slope.

The sixth-level and seventh-level slopes were protected by a trapezoidal frame and a three-dimensional net and vegetation, respectively, without any other anchoring measures taken for the slope soil. Therefore, the slope soil could slide along the potential sliding surface. Anchors are a passive protective measure to prevent slope movement trends. While anchoring the fifth-level slope to resist sliding, a stress concentration zone was generated at the foot of the slope. The closer the anchor is to the foot of the slope, the greater the load stress it receives. The test results of load stress and their changes are consistent with this point. Based on this trend, it can be inferred that there was a trend of bulging and sliding

along the foot of the slope on the fifth-level slope, where the stress was the highest, and the tension stress of the anchor closest to the foot of the slope was also the highest.

Figures 6 and 7 show the stress variation in anchor rods 1 and 2 located in the first-level slope. The monitoring results of tensile stress on anchor rods 1 and 2 in the first-level slope fluctuated within the range of a zero-stress load position, with a fluctuation range within 2 kN for anchor rod 1 and within 1 kN for anchor rod 2. Therefore, it can be inferred that during the entire slope reinforcement and construction phase to the stable operation phase, the first-level slope remained in a state of basic stability, with no significant stress being generated in the slope.
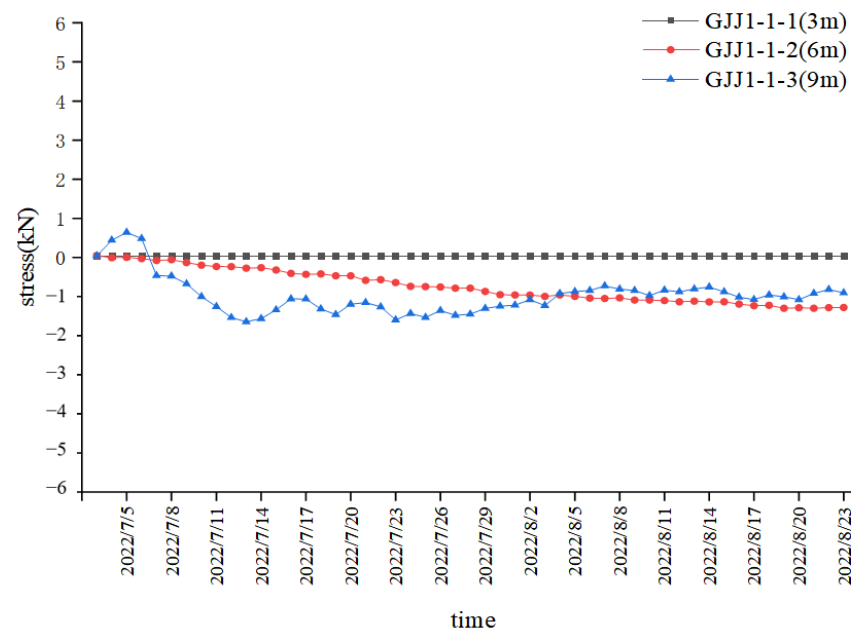

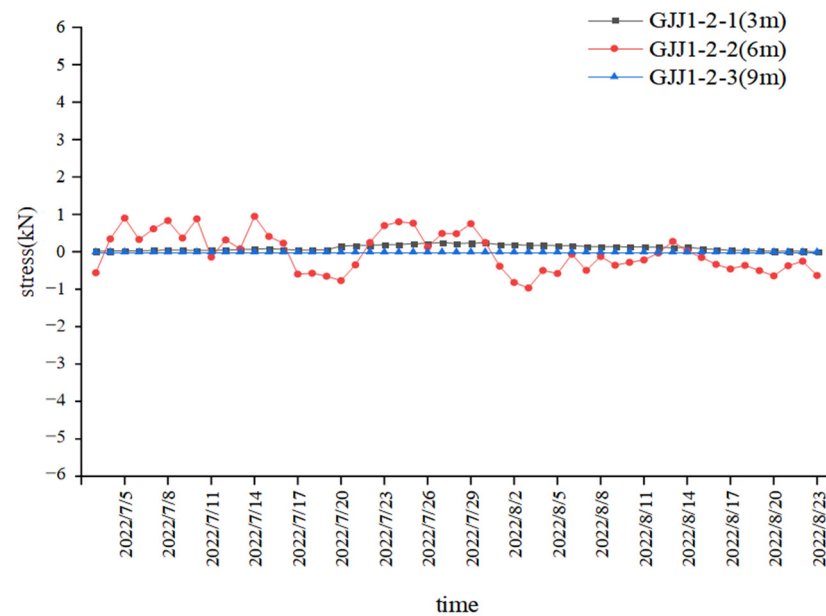**Figure 6.** No. 1 Anchor Bolt of the First Slope.

Figure 7. No. 2 Anchor Rod of the First Slope.

The slope ratio of the first- and second-level slopes was 1:0.75, which is greater than that of the other level slopes. The third- and fourth-level slopes were anchored with 25 m

long anchor cables, while the first-, second-, and fifth-level slopes were anchored with 12 m long fully bonded anchor rods. The combination of these two anchoring measures ensured the overall stability of the slope and fully utilized the self-supporting capacity of the slope. Therefore, there was no significant stress concentration zone in the first-level slope, and the tensile stress of the anchored anchor rods was relatively small, which is consistent with the monitoring data results.

The third- and fourth-level slopes were located in the middle section of the entire deep excavation slope, requiring the most robust and reliable protective measures. They were anchored with 25 m long anchor cables, and the length of the anchored segment was 13 m.

Figure 8 presents the stress variation in the anchor cables for the third-level slope. The maximum tensile stresses of the three anchor cables from bottom to top for the third-level slope were 40.997 kN, 173.110 kN, and 40.668 kN, respectively. For the fourth-level slope, the maximum tensile stresses of the three anchor cables from bottom to top were 146.927 kN, 246.560 kN, and 143.257 kN, respectively.
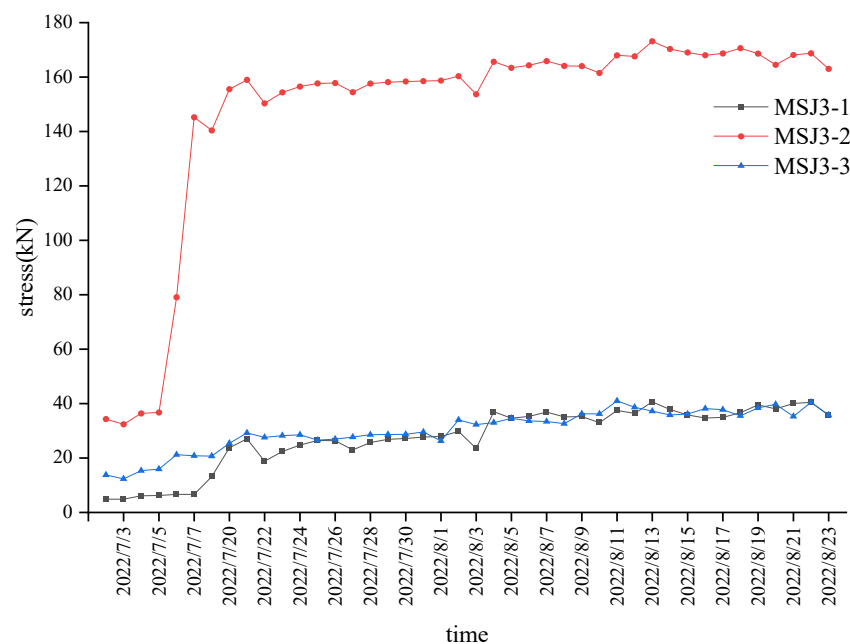

Figure 8. MSJ Stress of the Third Slope.

The stress monitoring data curves of the first and third anchor cables for the third-level slope are closer, and their tensile stresses gradually increased at a slower rate until they reached a stable state. During the operation and maintenance phases of the slope, the tensile stresses of the first and third anchor cables were both close to 40 kN. The stress monitoring data of the second anchor cable remained in a stable zone around 38 kN during the initial three days of tensioning. On 5 July 2022, a turning point marked the beginning of a steep increase in tension stress for the second anchor cable, while the turning point marking the end of this steep increase in tension stress was on 7 July 2022. This is due to the sharp increase in stress on the support structure caused by the start of slope construction on 5 July. The tensioning stress of the second anchor cable gradually stabilized and reached around 170 kN during the operation and maintenance phase.

Figure 9 shows the stress variation in the anchors on the fourth-level slope. After the three anchors on the fourth-level slope were installed and monitored, the monitoring data of the anchor tension stresses were relatively stable during the first four days. The anchor closest to the slope toe, anchor 1, had the maximum measured tension stress, approaching 50 KN, followed by anchor 3, with a tension stress of 30 kN, while anchor 2 had a tension stress measurement value of only 10 kN. The 5 of July was the inflection point of the anchor tension stress monitoring value, after which the anchor tension stresses entered a steep rise

stage. The 7 of July was the inflection point marking the end of this steep rise stage, after which the tension stresses of the three anchors gradually stabilized and entered a stable stage. After the construction phase was completed, the system entered the maintenance and later operation phase, during which the anchor tension stress monitoring data of the three anchors showed slight differences. From construction to the maintenance and operation phases, the tension stress of anchor 1 gradually approached 140 kN, while the tension stress of anchor 2 increased further and stabilized at around 240 kN, and the tension stress of anchor 3 gradually stabilized and approached 140 kN.
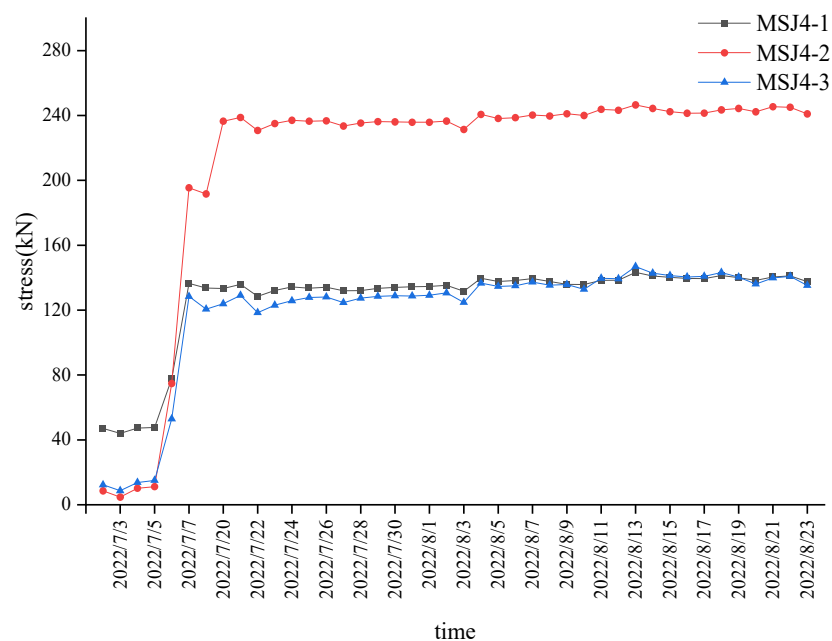

Figure 9. MSJ Stress of the Fourth Slope.

The monitoring data of the anchors on the third- and fourth-level slopes corresponded precisely with the casting time of the anchor frame beams during the steep rise stage. After the construction of the frame beams was completed and had achieved a certain strength, the stability of the slope was further improved, and the deformation trend of the slope body was effectively inhibited, with the internal stress of the anchors gradually stabilized. This change trend corresponds to the change trend of the monitoring data of the anchor tension stresses.

From the monitoring data of the anchor tension stresses on the third- and fourth-level slopes, it can be inferred that the tension stresses of the anchors stabilized by the maintenance and operation phase, and all the maximum anchor tension stresses were located in the middle of the slope where the anchors were fixed. It can be speculated that the third and fourth-level slopes were not primarily deforming by sliding along a potential slip surface near the slope toe, but by the bulging deformation of the slope body, with the middle position of the slope undergoing a larger deformation, and the anchor tension stresses being correspondingly larger in this position. According to the monitoring data of the tension stress of the anchor cable of the third- and fourth-level slopes, the tension stress of the anchor cable became stable during the maintenance operation stage, and it was largest for the anchor cable at the middle position of the slope. This was precisely caused by the expansion and deformation of the slope body.

5. Numerical Simulation Analysis

5.1. Numerical Method

An anchor cable is a one-dimensional structural element that provides axial tensile resistance but cannot provide bending resistance. The axial force produced by the anchor cable is calculated by measuring the displacement along the reinforced axial nodes. The

imbalance force at each node is due to its axial force and the tangential force along a cement slurry ring. The axial displacement is then calculated based on the acceleration caused by the imbalance in axial force at each node and the concentrated mass of the node. The interface deformation between the anchor cable and the rock mass is essentially due to adhesion and friction. The anchor cable tray was simulated by fixing the anchor cable end in the XYZ-direction with six degrees of freedom, including translational and rotational movement. A pre-stress of 550 KN was applied to the free section of the anchor cable as required by the design documents.

To simulate the anchor rod, a three-dimensional pile element was established using FLAC3D. Special command (structural pile property rockbolt flag on) streams needed to be called in to make the pile yield in the axial direction. The yield strength parameter needed to be set separately, and the tensile failure deformation value was also custom-defined to determine whether the anchor rod was broken. The constraint stress around the support, the strain softening characteristics between the pile and the mesh, and the pile's fracture could then be calculated. The shear and normal characteristics between the contact surface of the pile and mesh naturally adhered and were frictional.

The beam structure element consisted of two straight-line segments with the same symmetrical cross-section between two nodes. It is a three-dimensional structural element with isotropic, linear elastic material that does not yield. It can withstand forces, moments, and bending. The beam has 12 degrees of freedom at both ends, and the ultimate plastic moment can be specified. The interaction between the anchor cable (anchor rod) and the frame beam element, as well as their interaction with the rock and soil, was achieved through connections. There are three types of connections: free connection (the node velocity is independent of its connection body), rigid connection (the node and the connection body are connected together, and their velocity is the same), and deformable connection (the relationship between the node and the connection body is followed by a connecting spring). The transfer of force between each component was achieved through connections, thereby achieving interaction.

5.2. Model Establishment

The slope model was established using Rhino 6.0 software, as shown in Figure 10. After the model was established, the grid was divided by the grid division function, and then the grid was exported to the grid file recognized by FLAC3D (FLAC3D is a commonly used numerical analysis software in geotechnical engineering. There are many constitutive models of soil and rock in this analysis software, and its computational performance is superior, making it suitable for the relevant analysis in this paper). Finally, the simulation calculation was carried out in FLAC3D software.
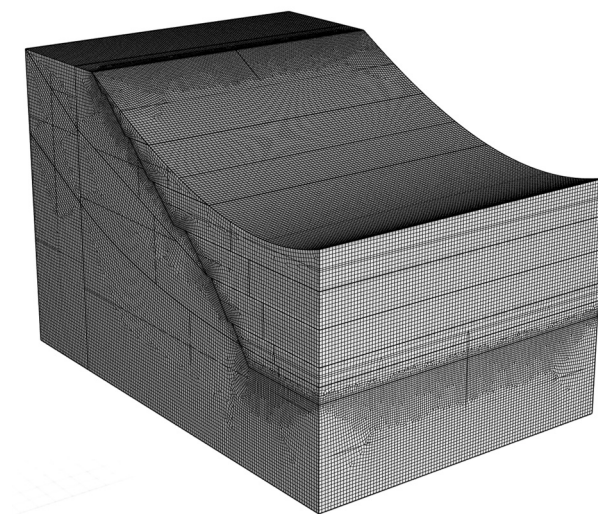

Figure 10. Slope Grid Model.

5.3. Essential Parameters

The model has a total length of 146.2 m, height of 95.1 m, and width of 130 m. It consists of 2,495,142 elements and 2,070,370 nodes. The rock, soil, and anchor rods in the slope were both modeled using elastic–plastic methods, and the left, right, and bottom boundaries of the model were fixed in numerical simulations. Displacement boundary conditions were employed, where the X boundary was constrained in the X-direction while allowing free deformation in other directions, and the Y-boundary was constrained in the Y-direction while allowing free deformation in other directions. The bottom boundary was fixed to restrict its deformation, while the top surface had a free boundary. The Mohr–Coulomb constitutive model was used to simulate the rock and soil materials of the slope, with the parameters for the slope materials shown in Table 1 based on laboratory tests and design data. Figure 11 shows the natural slope model, while Figure 12 illustrates the frame beams of the anchored rods and anchor cables.
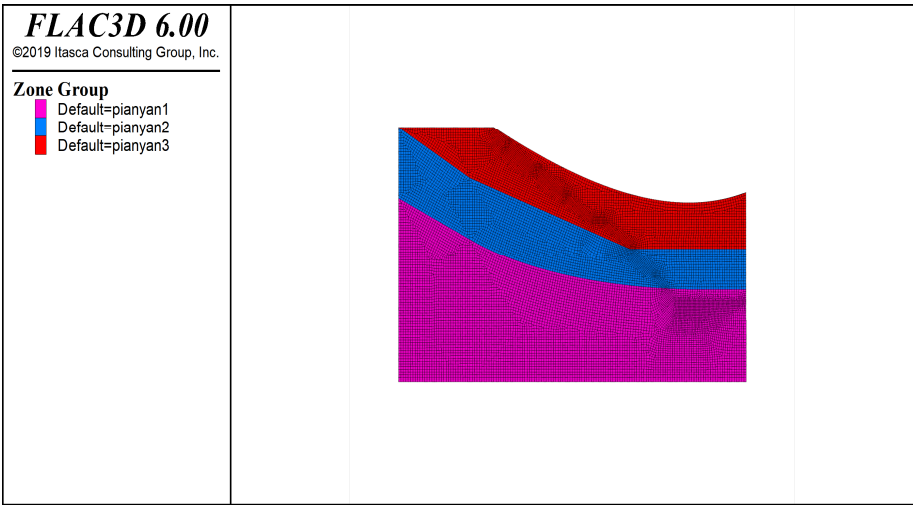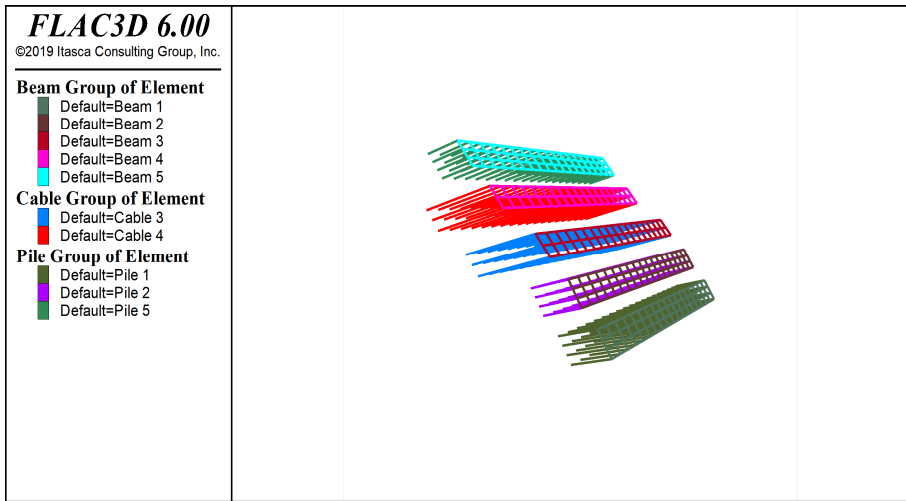

Figure 11. Natural slope model.

Figure 12. Anchor Cables and Anchor Frame Beams.

5.4. Numerical Simulation Result Analysis

The pre-excavation parameters of the slope were assigned to generate the initial stress field under the action of gravity. Two scenarios were simulated during the modeling process: (1) staged excavation, where each stage of the slope was excavated and calculated for stress equilibrium before proceeding to the next stage, and (2) staged excavation with

support, where each stage of the slope was excavated and supported with anchor rods or anchor cable frame beams before calculating stress equilibrium and proceeding to the next stage until the excavation and support of the entire slope were completed. Displacement monitoring points were set on the slope surface at each stage of the excavation, mainly to monitor the X-direction displacement (in the direction of the excavated face) of the slope surface, while also monitoring the axial force of the anchor rods and anchor cables. The location of the monitoring points is shown in Figure 13.
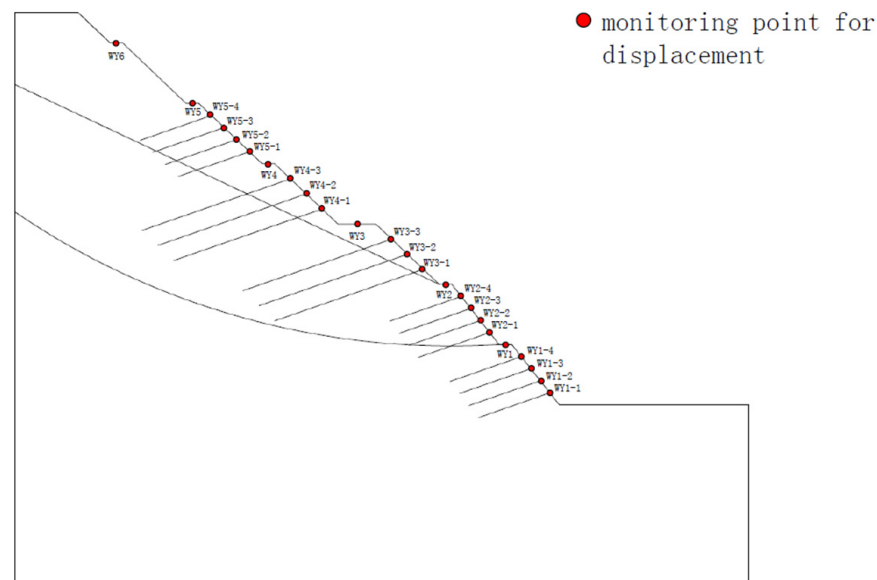

Figure 13. Monitoring Point for Displacement.

(1)   Shear Strain Increment Analysis

Under the self-weight of gravity of the rock slope, the shear strain increment was small. The maximum shear strain increment of the slope without support under the staged excavation conditions was 9.64×10^{-4}, and that under the staged excavation and support conditions was 9.02×10^{-4}. The maximum shear strain increment occurred at the toe of the first-level slope after excavation, as shown in Figures 14 and 15. At the toe of the fifth-level slope, the shear strain increment was 2.61×10^{-4} without support and 2.34×10^{-4} with support, reduced by 0.27×10^{-4}. At the toe of the fourth-level slope, the shear strain increment was $3.24c \times 10^{-4}$ without support and 3.03×10^{-4} with support, reduced by 0.21×10^{-4}. At the toe of the third-level slope, the shear strain increment was 4.41×10^{-4} without support and 3.14×10^{-4} with support, reduced by 1.27×10^{-4} mm. At the toe of the second-level slope, the shear strain increment was 6.40×10^{-4} without support and 5.70×10^{-4} with support, reduced by 0.70×10^{-4}. At the toe of the first-level slope, the shear strain increment was 9.64×10^{-4} without support and 9.02×10^{-4} with support, reduced by 0.62×10^{-4}. The data indicate that the shear strain of the slope increased as the excavation proceeded, indicating that the stability of the slope weakened as the excavation depth increased. The second- and third-level slopes were supported by anchor frames, while the first-, fourth-, and fifth-level slopes were supported by anchor rods and frames. The reduction in shear strain after support by anchor frames was greater than that after support by anchor rods and frames, indicating that the support effect of anchor frames is better than that of anchor rods and frames. Choosing anchor frames for support near the toe of a slope after excavation can better improve the stability of the slope.
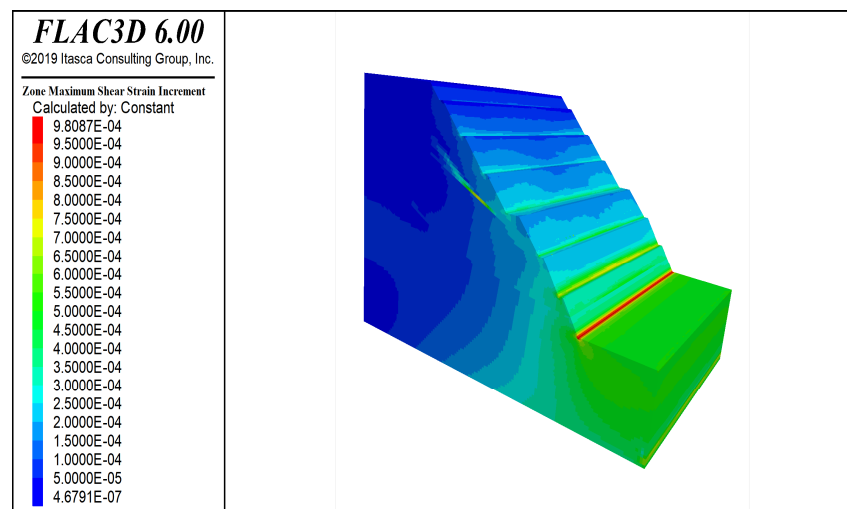
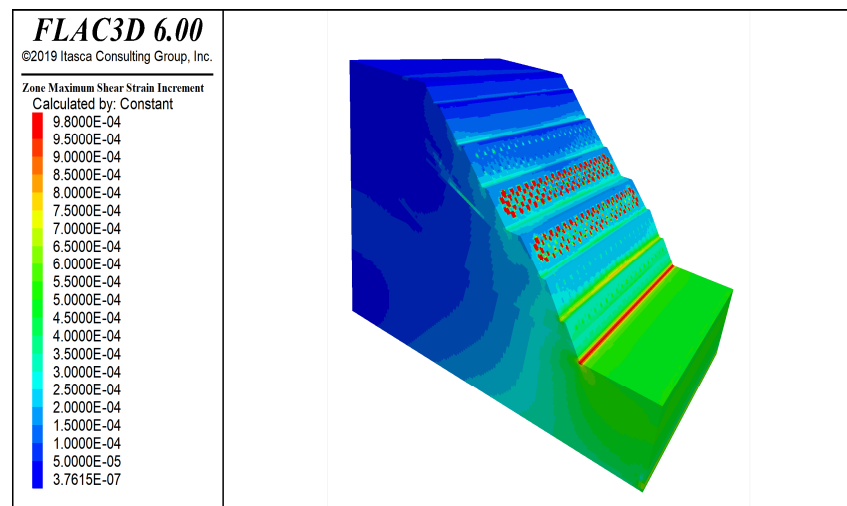**Figure 14.** Unsupported Shear Strain Increment after Slope-Grading Excavation.

Figure 15. Shear Strain Increment after Grading Excavation and Support of the Slope.

(2)   Displacement Analysis

As shown in Figure 16, the X-direction displacements of the monitoring points on the slope surface after staged excavation are presented. The displacement of monitoring points varied with the number of calculations, and displacement converged after each excavation. The calculation shows that the slope maintained stability with each excavation. As shown in (a), the displacement increased with the excavation of the slope, and the displacement rate accelerated. For the deep excavation slope of the road cut, after the upper soil was excavated, the slope surface rebounded toward the empty space under the initial stress field. The smaller the amount of excavation soil, the smaller the rebound displacement, as shown in (f). The maximum X-direction displacement of the fifth-level slope surface was 0.5 mm, and that of the first-level slope surface was 3 mm. Although the slope surface displacement slightly decreased after excavation, it continued to increase under the sliding force of the upper soil. As shown in (b), the maximum displacement of WY1–3 was 0.3 mm and located in the middle position of the first-level slope, where the sliding surface may have slid out. However, the maximum displacement of the slope was 0.3 mm, and it is currently in a stable state.
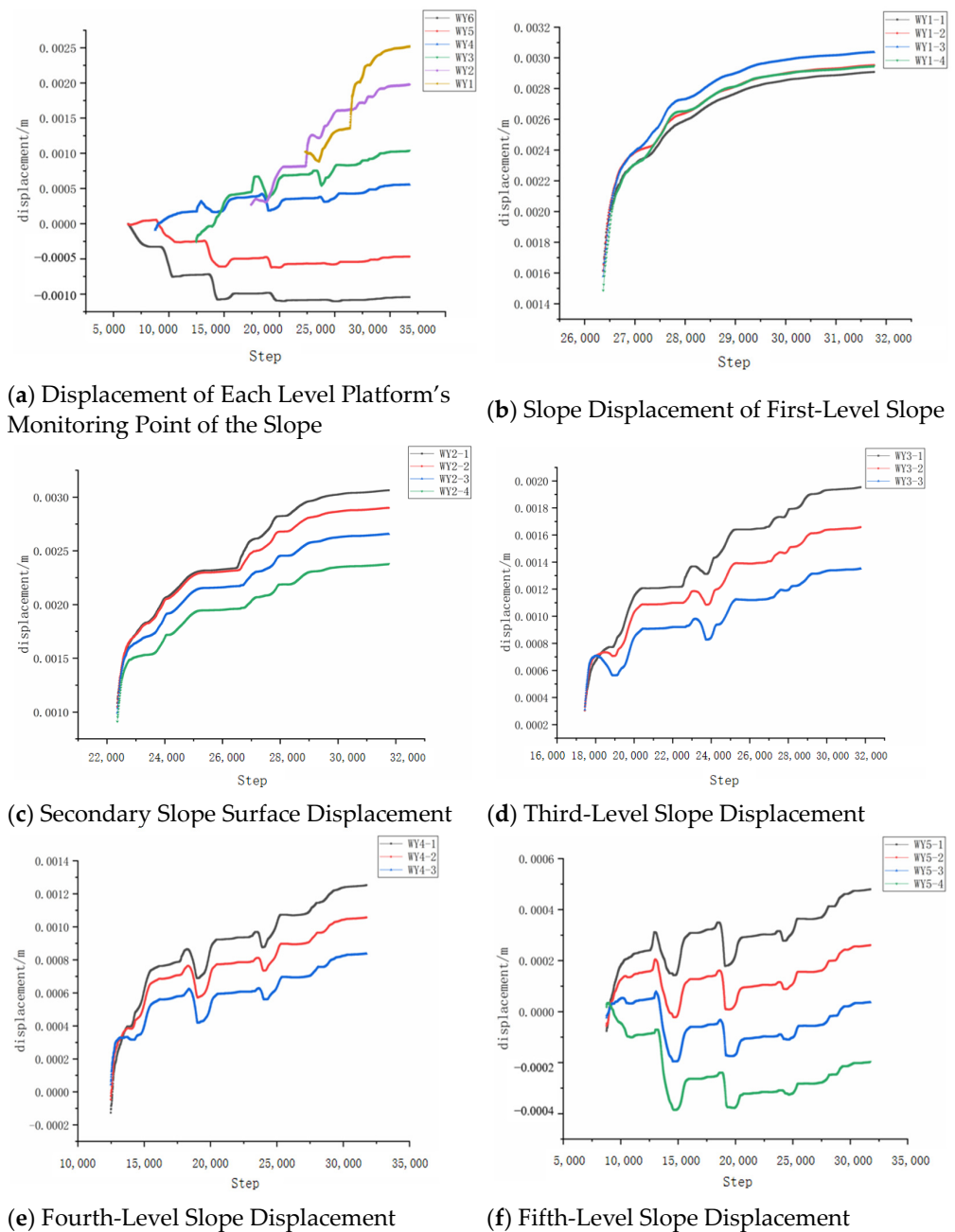
(a) Displacement of Each Level Platform's Monitoring Point of the Slope

(b) Slope Displacement of First-Level Slope

(c) Secondary Slope Surface Displacement

(d) Third-Level Slope Displacement

(e) Fourth-Level Slope Displacement

(f) Fifth-Level Slope Displacement

Figure 16. Slope Grading Excavation Unsupported Displacement of Each Monitoring Point.

As shown in Figure 17, the change trend of X-direction displacement on the back slope of the slope after support was the same as that before support. The slope was strengthened in terms of shear resistance and integrity after being supported by anchor rods and anchor beam frames, resulting in varying degrees of reduction in the displacement of each level of the slope surface. The maximum difference in slope surface displacement between supported and unsupported conditions for the first- to fifth-level slopes was 0.62 mm, 0.7 mm, 1.27 mm, 0.21 mm, and 0.27 mm, respectively. The displacement reduction under the action of anchor beam frames was greater than that under the action of anchor rods, indicating that the reinforcement effect of the anchor beam frame is better than that of the anchor rod frame.
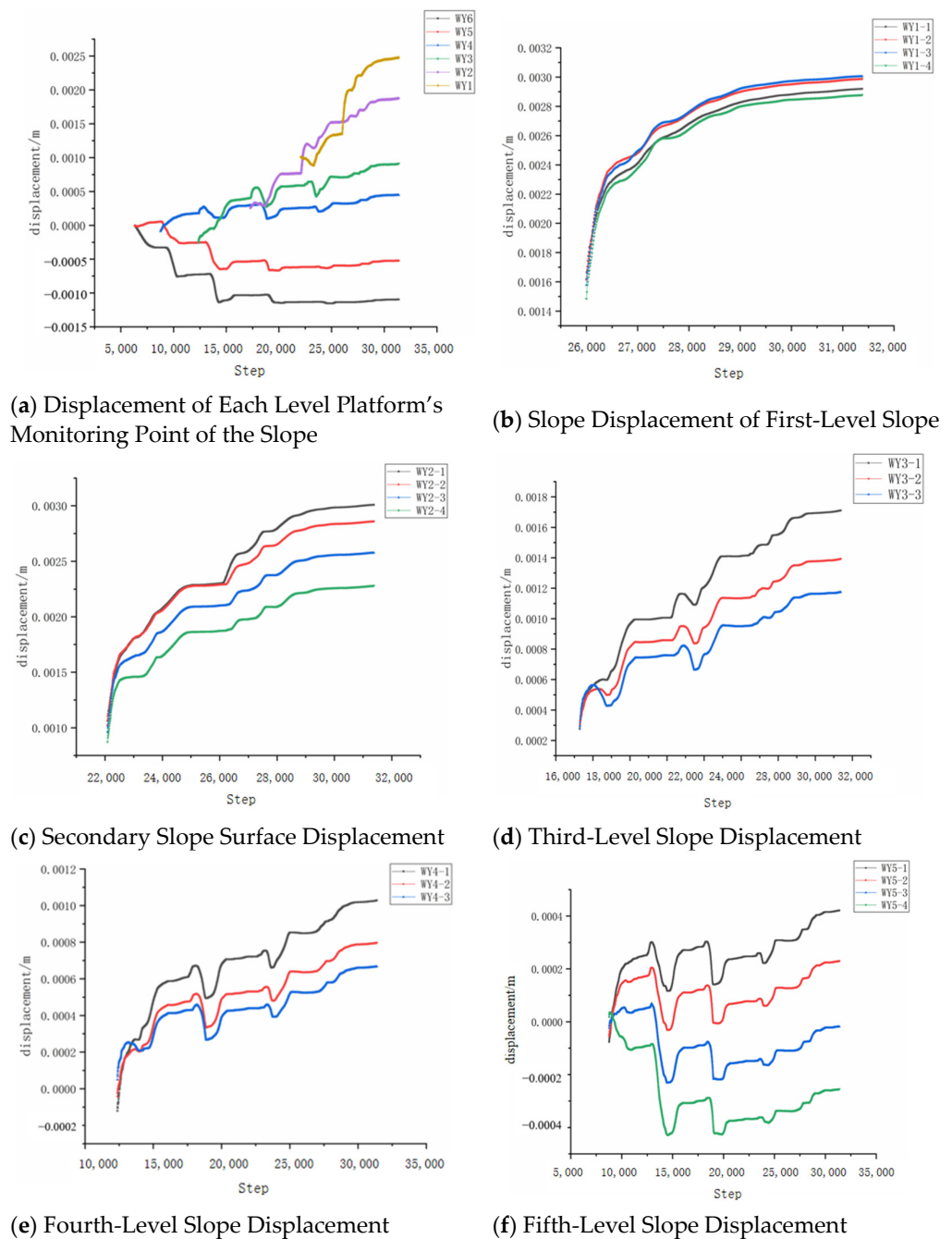
(**a**) Displacement of Each Level Platform's Monitoring Point of the Slope

(**b**) Slope Displacement of First-Level Slope

(**c**) Secondary Slope Surface Displacement

(**d**) Third-Level Slope Displacement

(**e**) Fourth-Level Slope Displacement

(**f**) Fifth-Level Slope Displacement

Figure 17. Displacement of Each Monitoring Point after Grading Excavation and Support of Slope.

In order to better evaluate the stability coefficient of the supporting slope, in this article, we adopted the strength reduction method for calculation. In the strength reduction method, the slope is made to turn into the limit equilibrium state by reducing the shear strength of soils, and the reduction factor *k* is the safety factor. The following equation was used for this calculation:

$$c' = c/Fs, \varphi' = arctan(tan\varphi/Fs)$$

where *Fs* is the reduction factor, *c* is the cohesion, φ is the angle of internal friction, and *c'*, φ' are the numerical values of *c* and φ after reduction, respectively.

After calculation, the stability coefficient of the slope reached 3.53, meeting the requirements of the specifications.

6. Conclusions

This paper presents the deformation distribution of a slope during excavation and the stress situation of anchor rods, which have a good enlightening effect on the development of related engineering. The main conclusions of this paper are the following:

1. In the treatment and protection of high slopes, the slope is classified based on the engineering geology and hydrological conditions, the design stress of the slope, and the actual construction conditions, and then economically reasonable support and protection measures are taken for each level of the slope while ensuring stability and safety.

2. According to the monitoring data of the slope analyzed in this study, it can be concluded that the slope is in a stable state with dual protection of anchor rods and anchor cables, and there has been no significant mutation point in the structural stress of the anchor rods and anchor cables. This is because the anchor rods and anchor cables can withstand large sliding forces and ensure the stability of the slope.

3. Based on FLAC3D simulation and monitoring point settings, it was found that for the deep excavation of the road-cutting slope, after the rock and soil were excavated, the slope surface rebounded under the action of the initial stress field, and the rebound increased with the increase in the excavation volume. According to the shear strain increment cloud map, it can be seen that sliding occurred at the interface of the upper rock layer, indicating the need to strengthen protection at the interface of the rock and soil. For the deep excavation of the road-cutting slope, the reinforcement effect of the anchor cable frame beam was stronger than that of the anchor rod frame beam. Therefore, the anchor cable frame beam should be used for reinforcement at locations where sliding deformation is greater at the bottom of a slope.

References

1. Yongfu, X.; Yan, C.; Jie, X.; Yuliang, L.; Shunchao, Q. New prevention and control technology for expansive soil slopes. *Chin. J. Geotech. Eng.* **2022**, *44*, 1281–1294.
2. Linfeng, W.; Wangchun, X.; Lang, X.; Huang, X.-M.; Tan, G.-J.; Zhang, J.-X. Structure and seismic performance analysis of plate spring damping anchor head. *J. Jilin Univ.* **2023**, *53*, 1842–1852. [CrossRef]
3. Li, Z.; Zhenyu, Z.; Lixuan, L.; Chao, L.; Xin, L.; Shumao, Q. Design parameters optimization of micro-pile based on field test and numerical simulation. *J. Beijing Jiaotong Univ.* **2019**, *43*, 52–57.
4. Ziyao, M.; Zhijian, C.; Tao, C. High Rock Slope Anchor Bolt Axial Force Prediction Based on ACO-SVM Model. *Coal Geol. China* **2019**, *31*, 53–57.
5. Huang, Y.; Xu, X.; Mao, W. Numerical performance assessment of slope reinforcement using a pile-anchor structure under seismic loading. *Soil Dyn. Earthq. Eng.* **2020**, *129*, 105963. [CrossRef]
6. Jianhui, Y.; Zihang, D.; Zhijun, W. Simplified finite element computation of slope anchor frame considering influence of friction resistance and axial loads. *China Civ. Eng. J.* **2023**, *56*, 116–125+146. [CrossRef]
7. Minggang, S.; Xin, X.; Guangcheng, Z.; Wang, Q.; Zheng, J.; Li, H.; Qui, X. Study on the mechanical characteristics and prestress loss of slope-anchored structure. *Chin. J. Rock Mech. Eng.* **2022**, *41* (Suppl. S1), 2791–2800. [CrossRef]
8. Zhikai, Y.; Kunlin, L.; Feng, S.; Da-Yong, Z. Optimization of anchorage location of three dimensional slopes based on improved differential evolution algorithm. *Chin. J. Geotech. Eng.* **2020**, *42*, 1322–1330.

9.   Zhixin, Y.; Chunbo, L.; Zhe, L.; Yang, H.; Ruixiang, L.; Gonghui, Z. Anchorage deformation of bedding rock slope with weak layer under earthquake loading. *J. Vib. Eng.* **2020**, *33*, 1302–1312. [CrossRef]

10.   Xiuqing, C.; Baoyu, W.; Jinlong, W.; Fei, Y. Secondary Reinforcement Measures of Anti-slide Piles in a Slope Treatment Engineering in Xujiawan, Lanzhou. *Saf. Environ. Eng.* **2023**, *30*, 166–173. [CrossRef]

11.   Qiu-Yi, W.; Yao-Ming, T.; He-Fen, Y.; Hong, Y.; Hong-Gang, W. Study on Dynamic Response Law of High Weathered Basalt High Slope Strengthened by BRFP Anchor Cable Frame. *Value Eng.* **2019**, *38*, 132–137.

12.   Feng, J.; Chen, J.; Li, J.; Zhang, J.; Guo, J.; Qui, H. An early warning method for a slope based on the increment ratio of anchor cable internal force. *Arch. Civ. Eng.* **2023**, *69*, 553–569.

13.   Xu, X.; Xing, Y.; Guo, Z.; Huang, Y. Stability Analysis of Rainfall-Triggered Toe-Cut Slopes and Effectiveness Evaluation of Pile-Anchor Structures. *J. Earth Sci.* **2021**, *32*, 9. [CrossRef]

14.   Yongfu, X.; Yan, C.; Tang, H. Failure characteristics of expansive soil slope and standardization of slope slide prevention by geotextile bag. *J. Cent. South Univ.* **2022**, *53*, 1–20.

15.   Wuchao, W.; Shaorui, S.; Jihong, W.; Yong-Xiang, Y.; Wei, H.; Jing-Jei, S. Numerical experimental study on optimum design of anchorage system for Xiashu loess slope. *J. Cent. South Univ.* **2021**, *28*, 2843–2856.

16.   Bingli, G.; Jinhou, Z.; Xiaohui, L.; Haixing, Z.; Chanoyang, Y. Stability analysis and prevention measures of rock slope in mountain scenic area. *J. Eng. Geol.* **2022**, *30*, 1316–1324. [CrossRef]

17.   Changgen, Y.; Zherui, L.; Zhuolong, J.; Heng-Xing, L.A.N.; Yu-Ling, S.S.; Wan-Li, Y.A.N.G. Review on surface protection technologies of loess slope. *J. Traffic Transp. Eng.* **2023**, *23*, 1–22. [CrossRef]

18.   Li, D.; Zhang, Z. The Anti sliding Mechanism of Adjacent Pile-Anchor Structure considering Traffic Load on Slope Top. *Adv. Civ. Eng.* **2021**, *2021 Pt 23*, 1–11. [CrossRef]

19.   Zhixin, Y.; Zhe, L.; Shen, Z.; Zhou, X.L.; Dong, J.H.; Jiang, P. Analysis of shear stress distribution at the anchorage interface of rock slope and its influencing factors under seismic action. *J. Vib. Eng.* **2019**, *32*, 1029–1040. [CrossRef]

20.   Nguyen, P.M.V.; Wrana, A.; Rajwa, S.; Różański, Z.; Frączek, R. Slope Stability Numerical Analysis and Landslide Prevention of Coal Mine Waste Dump under the Impact of Rainfall—A Case Study of Janina Mine, Poland. *Energies* **2022**, *15*, 8311. [CrossRef]

21.   Di Maio, C.; Fornaro, G.; Gioia, D.; Reale, D.; Schiattarella, M.; Vassallo, R. In situ and satellite long-term monitoring of the Latronico landslide, Italy: Displacement evolution, damage to buildings, and effectiveness of remedial works. *Eng. Geol.* **2018**, *245*, 218–235. [CrossRef]

22.   Dong, K.; Yang, D.; Chen, J.; Zhou, J.; Li, J.; Lu, X.; Kou, Q. Monitoring-data mechanism-driven dynamic evaluation method for slope safety. *Comput. Geotech.* **2022**, *148*, 104850. [CrossRef]

23.   Kumar, S.; Roy, L.B. Case study on soil-reinforced embankment slope stability with natural fibre additives. *Proc. Inst. Civ. Eng. Eng. Sustain.* **2023**, *176*, 270–284. [CrossRef]

24.   Tiwari, G.; Latha, G.M. Design of Rock Slope Reinforcement: An Himalayan Case Study. *Rock Mech. Rock Eng.* **2016**, *49*, 2075–2097. [CrossRef]

25.   Chen, J.; Du, C.C.; Qingzhao, Z.; Xiaopeng, G. A Case Study of Two Failures of a High Cut-slope in the Northeastern Area of Sichuan, China. *Res. Sq.* **2022**. [CrossRef]

26.   Urbański, A.; Grodecki, M. Protection of a building against landslide. A case study and FEM simulations. *Bull. Pol. Acad. Sci. Tech. Sci.* **2019**, *67*, 567–663. [CrossRef]

27.   Arbanas, Z.; Grošić, M.; Kovačevic, M.S. Rock Mass Reinforcement Systems in Open Pit Excavations in Urban Areas. In *Slope Stability 2007: In Proceedings of the 2007 International Symposium on Rock Slope Stability in Open Pit Mining and Civil Engineering, Australian Centre for Geomechanics, Perth, Australia 12–14 September 2007*; Potvin, Y., Ed.; Australian Centre for Geomechanics: Crawley, Australia; pp. 171–183. [CrossRef]